Indonesian Journal of Computing, Engineering, and Design

Journal homepage: http://ojs.sampoernauniversity.ac.id/index.php/IJOCED

Mechanical Properties Analysis on the Reduced Graphene Oxide/Silver Nanoparticle/Polylactic Acid Composites

Iwan Setiawan [1], Charlene Tiara Rehueliah Pingak [2], Amartya Natayu [2], Budi Hadisujoto [2], Murni Handayani [3]*

[1] Information System Department, Faculty of Engineering and Technology, Sampoerna University, Jakarta 12780, Indonesia

[2] Mechanical Engineering Department, Faculty of Engineering and Technology, Sampoerna University, Jakarta 12780, Indonesia

[3] Research Center for Advanced Materials – National Research and Innovation Agency (BRIN), Tangerang Selatan 15314, Indonesia

Corresponding email: iwan.setiawan@sampoernauniversity.ac.id

ABSTRACT

We present the characteristics and mechanical strength of rGO-AgNPs nanocomposites in PLA-based 3D printing. The nanocomposites are characterized using X-ray diffraction and UV-Vis spectroscopy. The XRD spectrum reveals diffraction peaks at 38.14°, 44.30°, 64.50°, and 77.42°, corresponding to the (111), (200), (220), and (3111) planes of the Ag crystals, respectively. Surface observations under the microscope for pure PLA and PLA rGO-AgNPs showed that the surfaces of the samples were uniformly distributed. The results of 3D printing indicated that the 0.10 g rGO-AgNPs nanocomposite particles were evenly distributed, although digital microscopy confirmed the presence of a few small particles that were not uniformly distributed. Tensile tests demonstrated that rGO-AgNPs exhibited higher tensile strength compared to pure PLA. Tensile strength increased as the quantity of rGO-AgNPs decreased. Young's modulus results, ranging from pure PLA to rGO-AgNPs, consistently showed an increase, with the highest Young's modulus measuring 7624.45 kPa. Therefore, specimens containing rGO-AgNPs displayed a greater modulus than others, indicating that rGO-AgNPs enhanced the mechanical properties of PLA-based 3D printing.

ARTICLE INFO

Article History:
Received 05 Sep 2023
Revised 12 Sep 2023
Accepted 12 Sep 2023
Available online 03 Oct 2023

Keywords:
Nanocomposites,
Reduced graphene oxide,
Silver nanoparticles,
Three-dimension scaffold,
Tissue engineering.

1. INTRODUCTION

Recently, graphene-based materials have garnered significant interest among

researchers due to their potential applications in biomedicine. These materials can be used independently or in conjunction with nanoparticles and polymers. Thanks to graphene's unique properties, it has been extensively explored as a platform for drug delivery in anti-cancer/gene therapy, biosensors, bioimaging, antibacterial applications, cell culture, and tissue engineering (Liu et al., 2013). The growing demand for organ and tissue transplants has led to increased research on cellular rejuvenation. Consequently, tissue and organ damage has given rise to a new technique known as tissue engineering.

Tissue engineering represents an alternative approach to current methods of bone regeneration and replacement therapy. Tissue-engineered bone constructs have the potential to reduce the need for bone augmentation materials, which are often in short supply, including suitable autograft and allograft materials (Shadjou et al., 2017). Furthermore, it aids in the regeneration of bodily tissues to address defects or injuries that cannot naturally heal (Bai et al.). Studies have reported that three-dimensional (3D) scaffolds hold promise as biomaterials for the future of tissue engineering (Sayyar et al., 2017; Bai et al., 2019; Silva et al., 2018). This approach can be employed to overcome the limitations of current conventional treatments. Scaffolds not only shield growing tissue from external stimuli but also collaborate with cells to enhance the bone growth response and promote tissue regeneration.

There are two techniques for scaffold fabrication: conventional and modern techniques. The conventional technique faces challenges in controlling the scaffold's geometry. To address this issue, researchers and engineers opted to develop the scaffold using additive manufacturing. Additive manufacturing (AM), also known as 3D printing or rapid prototyping, encompasses various techniques for transforming computer-aided design (CAD) models into three-dimensional objects constructed sequentially, layer by layer (Silva et al., 2018). Three-dimensional (3D) printing is a groundbreaking technique with significant potential in tissue and organ engineering, enabling the fabrication of 2D graphene into a 3D structure (Jakus et al., 2019). Further research on reduced graphene oxide (rGO), silver nanoparticles (AgNPs), and reduced graphene oxide-silver nanoparticles (rGO-AgNPs) is necessary to explore how these materials can be utilized to develop a suitable scaffold. The combination of rGO and AgNPs into rGO-AgNPs holds promise for tissue engineering.

Graphene, with its unique physical and chemical characteristics, has emerged as a promising biomaterial for biomedical applications, including tissue engineering, owing to its two-dimensional planar structure, large surface area, chemical and mechanical stability, superconductivity, and biocompatibility (Liu et al., 2013). In this study, graphene is the selected nanomaterial, benefiting from its distinctive attributes. Graphene's high surface area and the presence of free electrons make it an ideal platform for gene and drug delivery, while its mechanical and electrical conductivity make it valuable for bone and brain tissue engineering. Shin et al. have reported that graphene can interact with DNA, enzymes, proteins, and peptides, offering potential applications in regenerative medicine and tissue engineering (Shin et al., 2016).

Despite the interest in developing graphene-based materials as a tissue engineering application, there are still concerns about their toxicity, especially for the graphene-based 3D scaffold. Graphene's toxicity and its behavior in biological systems are fundamental issues that require significant attention. According to Singh, while graphene scaffolds hold great potential for future regenerative medicine

applications, concerns regarding their toxicity, biocompatibility, and biodegradability remain (Singh, 2016). Numerous studies have been conducted to assess the toxicological effects of graphene derivatives on biological models. Zheng et al. suggest that toxicological effects are influenced by various properties, including size, aggregation, chemical structure, crystal properties, and surface chemistry (Zheng et al., 2021). In this study, nanocomposites consisting of reduced graphene oxide (rGO) and silver nanoparticles (AgNPs) were used.

Reduced graphene oxide is a deoxygenated form of graphene oxide, commonly produced through chemical reduction methods. Using eco-friendly reducing agents is one strategy to mitigate potential toxicity. Silver nanoparticles (AgNPs) are known for their antibacterial properties against bacteria, viruses, and other eukaryotic microorganisms and have demonstrated antibacterial, antiviral, and antifungal effects, as reported by Fernando et al. (Fernando et al., 2018). The combination of AgNPs and rGO is expected to be beneficial, especially in bone tissue engineering as part of a scaffold. Therefore, this study aimed to investigate PLA-based 3D printing with reduced graphene oxide-silver nanoparticles (rGO-AgNPs) as nanofillers and nano-reinforcements.

The primary focus of this study is to synthesize and characterize reduced graphene oxide (rGO) and silver nanoparticles nanofillers and nano-reinforcements for PLA-based 3D printing, followed by conducting mechanical tests on the resulting samples.

2. RESEARCH METHODOLOGY

2.1. Synthesis of Graphene Oxide

The materials used in this study, namely graphite powder, sulfuric acid (H2SO4), sodium nitrate (NaNO3), potassium permanganate (KMnO4), hydrogen peroxide (H2O2), and ascorbic acid, were used as-is without further purification. The equipment employed in this study included a centrifuge (Labtron LS-A20), digital balance (Kern ABJ 220-4NM), furnace (Cress Furnace), and ultrasonicator (Brandson M3800). The graphene oxide used in this study was synthesized using the Hummers' method (Handayani et al., 2021; Affi et al., 2023).

2.2. Synthesis of Reduced Graphene Oxide-Silver Nanoparticles

2.2.1. Materials and Method

The reduced graphene oxide-silver nanoparticle was synthesized using a previously synthesized 0.25 mg/mL GO solution and 5 mL of 5 mM silver nitrate (Handayani et al., 2022; Ciptasari et al., 2022). The mixture was then sonicated for 30 minutes. After sonication, 7 mL of 1 M sodium hydroxide was added to the mixture, creating a gray black colored mixture. The mixture was then microwaved for 10 minutes and dried in the furnace at 60 degrees Celsius for 12 hours. The dried mixture was subsequently measured using a UV-vis spectrophotometer.

2.3. Digital Light Processing 3D Printing

The 3D printer used in this project was a DLP (Digital Light Processing)-type printing system (DLP Moonlite Printer). The resin used was Bio PLA Resin Pro transparent. The DLP-3D printer was used to fabricate graphene oxide/silver nanoparticles in PLA-based 3D printing specimens. Two types of printed specimens were produced for each material: the dog-bone specimen, as illustrated in **Figure 1**, and the cylindrical specimen, as illustrated in **Figure 2**. The dog-bone specimen was used for tensile strength testing, while the cylindrical specimens were observed for surface morphology. They may also be utilized for antibacterial testing in the future.

Figure 1. The dog-bone specimen design

Each of the reduced graphene oxide-silver nanoparticle mixtures was sonicated and then combined with 150 mL of PLA, followed by stirring. After stirring, each reduced graphene oxide-silver nanoparticles mixture turned black in color. These mixtures were then printed using the 3D printing machine.

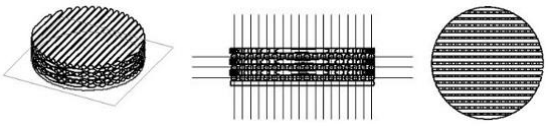

Figure 2. The cylindrical-shape specimen design

3. RESULT AND DISCUSSION

3.1. Materials Characterization

UV-Visible Analysis of rGO-AgNPs nanocomposites

Figure 3 displays the UV-visible spectra of the synthesized reduced graphene oxide-silver nanoparticles (rGO-AgNPs). The UV spectra of rGO-AgNPs exhibit two absorption peaks at 251.5 nm and 416 nm, characteristic of rGO and AgNPs, respectively. The wavelength of silver nanoparticles in this range varies based on their method, structure, and dimensions.

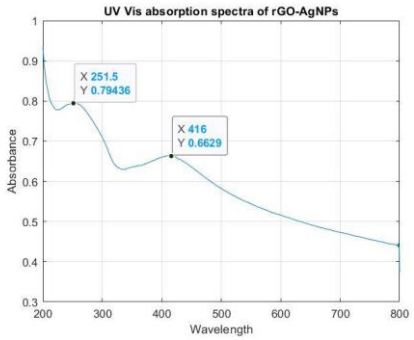

Figure 3. UV-Vis spectra of rGO-AgNPs (reduced graphene oxide-silver nanoparticles)

3.1.1. XRD Analysis of rGO-AgNPs nanocomposites

The XRD spectrum data obtained from the XRD test illustrates the correlation between the scattering angle (2θ) and the peak intensity (I), as depicted in **Figure 4**. A 2θ range of 5°–90° was used with Cu-Kα radiation (1.541862 Å). The dataset comprises X-ray diffraction intensity and 2θ values. This XRD analysis was performed on samples of reduced graphene oxide-silver nanoparticles (rGO-AgNPs). The formation of rGO-AgNPs was validated by the presence of a crystal structure diffraction pattern, in accordance with the JCPDS (Joint Committee on Powder Diffraction Standards), now known as ICDDS (International Centre for Diffraction Standards).

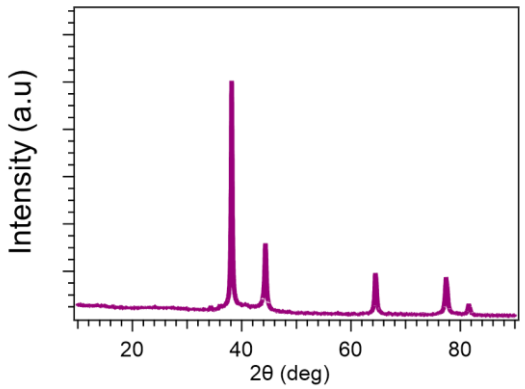

Figure 4. XRD spectra of rGO-AgNPs

The crystallinity of rGO-AgNPs was confirmed through XRD analysis, as depicted in **Figure 4**. Subsequently, the Full Width at Half Maximum (FWHM) value of the highest peak was determined and used to calculate the average crystallite size, also known as particle size, employing the Debye-Scherrer formula. The Debye-Scherrer method is a straightforward approach for measuring crystallite size by analyzing peak broadening, as shown in the formula below (Basak et al., 2022). Therefore, the crystallite size of rGO-AgNPs is presented in **Table 1**.

$$D = \frac{K\lambda}{\beta \cos\theta} \quad (1)$$

where:
D = Crystallite size (nm)
K = 0.9 (Scherrer constant)

Λ = 0.1541862 nm (wavelength of the X-ray sources)
B = full-width half maximum (FWHM, in radians)
Θ = peak position (in degrees)

In the nanocomposites of rGO/AgNPs, AgNPs have undergone further transformation into crystalline rGO-AgNPs, as evidenced by the more pronounced peak of AgNPs compared to that of rGO. This difference is due to the much higher crystallinity of AgNPS compared to rGO. The XRD spectrum reveals diffraction peaks at 38.14°, 44.30°, 64.50°, and 77.42°. These peaks can be attributed to the (111), (200), (220), and (3111) planes of the Ag crystals, respectively.

3.2. Samples Observation using a Microscope

The 3D results obtained using a DLP 3D printer were observed using the digital microscope VHX-7000 with high resolution and automatic zoom from 20x to 6000x. The lens used to observe the specimens was VHX-E500 with a magnification of 500x. The image size is 4000 x 3000. Therefore, the resolution at the above magnification is 0.1525 µm. **Figure 5** shows the specimens for pure PLA. When observed with the naked eye, PLA is uniformly mixed; however, when viewed at 500x magnification, small flakes are visible, likely caused by various external factors. These external factors can occur during the process of placing specimens or cleaning the DLP 3D printer after usage.

Table 1. Crystallite Size using Debye-Scherrer

	Peak Position (2θ)	Lattice Planes	FWHM	Crystallite Size, in nm	Average Crystallite Size, in nm
rGO-AgNPs	38.14715	(111)	0.34993	24.04096151	19.44506428
	44.30785	(200)	0.5844	14.68952639	
	64.48697	(220)	0.46018	20.42777827	
	77.42107	(311)	0.54716	18.62199094	

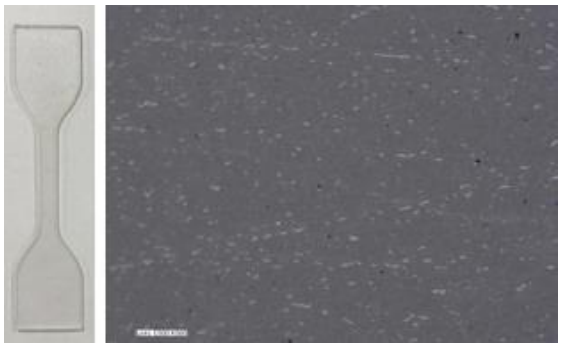

Figure 5. Specimen of Pure PLA and digital microscope image

In **Figure 6**, the mixing of 0.10 g rGO-AgNPs in each specimen appears to be uniformly spread, although some smaller flakes are still present.

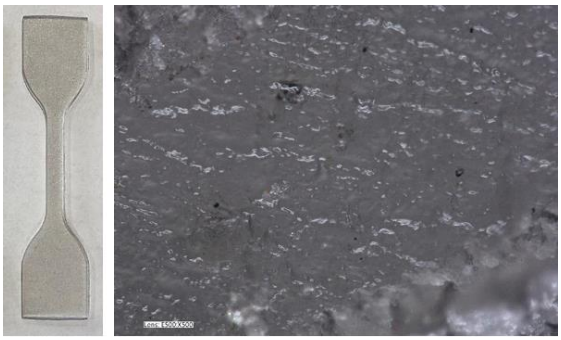

Figure 6. Specimen of 0.10 gr rGO-AgNPs and digital microscope image

Figures 7 and Figure 8 illustrate the specimens of PLA containing 0.15 g and 0.20 g of rGO-AgNPs, respectively. The results show that the mixing in both specimens, both 0.15 g and 0.20 g, was not uniform, resulting in variations in brightness and darkness. This uneven distribution can be attributed to a combination of external and internal factors. Firstly, during the pulverization of rGO-AgNPs, some particles

may not have been perfectly smooth. Secondly, in the 3D printing process, the DLP printer continuously projects all layers of the 3D model and simultaneously cures each point. The color density of rGO-AgNPs + PLA can affect the DLP's ability to project light onto the resin. Additionally, the presence of small particles on the surface can be influenced by the cleanliness of the DLP printer before and after use, as well as how the specimens are stored.

Figure 7. Specimen of 0.15 gr rGO-AgNPs and digital microscope images for dark and light distribution

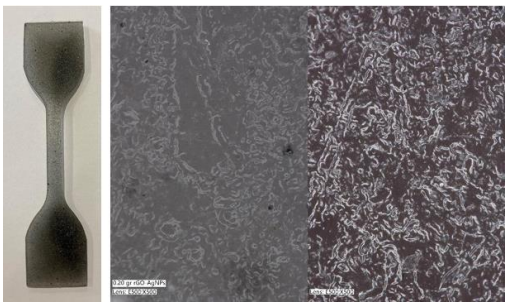

Figure 8. Specimen of 0.20 gr rGO-AgNPs and digital microscope images for dark and light distribution

Figures 9 - 12 depict the results obtained using a digital microscope for a cylindrical specimen of PLA (**Figure 9**) and rGO-AgNPs (**Figure 10 - 12**). The specimens were observed using two lenses: VHX-E20 with magnifications of 20x (resolution of 3.81 µm) and 50x (resolution of 1.525 µm), as well as VHX-E100 with magnifications of 150x (resolution of 0.5075 µm) and 300x (resolution of 0.255 µm). By employing microscopy for contamination analysis, it is possible to determine the extent of contamination resulting from the uneven distribution of each specimen.

According to the data obtained (**Table 2**), there were 16 contaminated areas in pure PLA, with a maximum size of 4.2 µm. Pure PLA specimens are not expected to contain any contaminated particles. As previously explained, during microscopy-based observations (**Figure 9**), a few small particles externally caused some contamination.

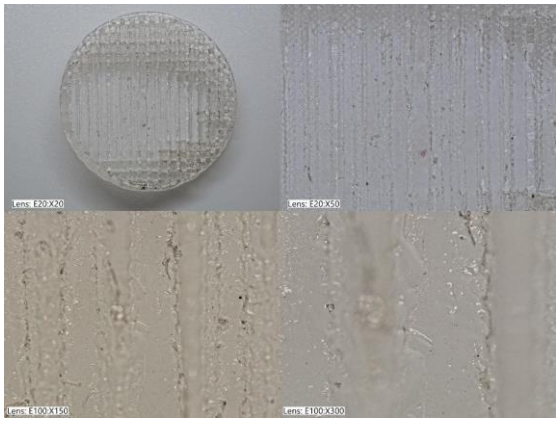

Figure 9. Digital microscope images of pure PLA

Table 2. Contamination analysis result in data of pure PLA

Interval	1	2	3	4	5	6	7	8	9	10
Max diameter (µm)	[0-5]	[5-15]	[15-25]	[25-50]	[50-100]	[100-150]	[150-200]	[200-400]	[400-600]	[600-]
Count	16	0	0	0	0	0	0	0	0	0

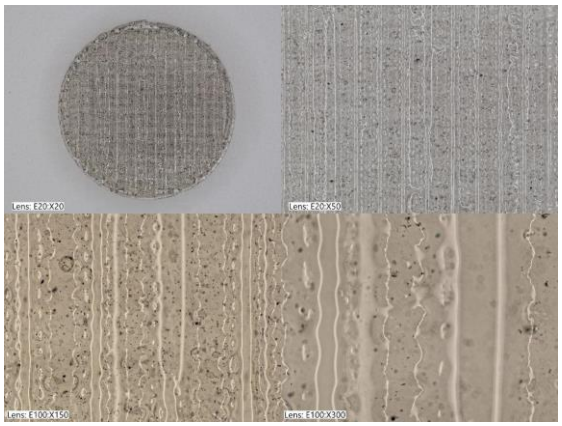

Figure 10. Digital microscope images of 0.10 gr rGO-AgNPs

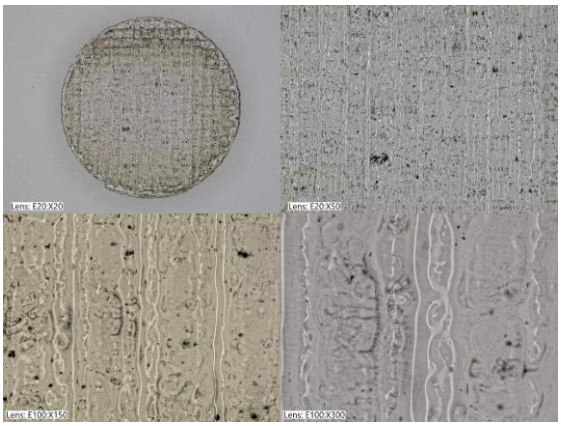

Figure 11. Digital microscope images of 0.15 gr rGO-AgNPs

Observations of contaminated areas and visuals were consistent for 0.10 g of rGO-AgNPs (**Figure 10** and **Table 3**), 0.15 g of rGO-AgNPs (**Figure 11** and **Table 4**), and 0.20 g of rGO-AgNPs (**Figure 12** and **Table 5**). There were 4891 contaminated areas for 0.10 g of rGO-AgNPs, with a maximum size of 219.1 µm. Additionally, there were 1706 contamination areas for 0.15 g of rGO-AgNPs, with a maximum size of 139.1 µm, and 5998 contamination areas for 0.20 g of rGO-AgNPs, with a maximum size of 260.3 µm.

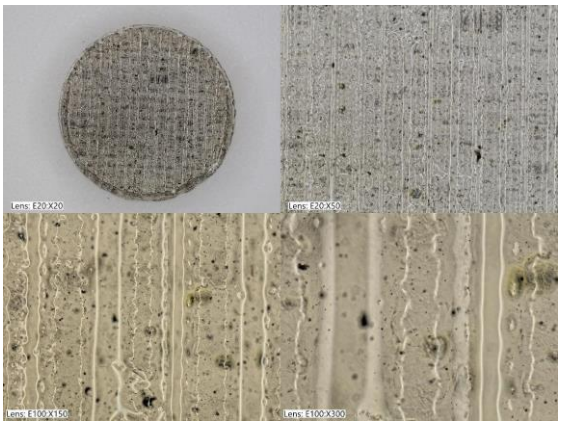

Figure 12. Digital microscope images of 0.20 gr rGO-AgNPs

Table 3. Contamination analysis result data of 0.10 gr rGO-AgNPs

Interval	1	2	3	4	5	6	7	8	9	10
Max diameter (µm)	[0-5]	[5-15]	[15-25]	[25-50]	[50-100]	[100-150]	[150-200]	[200-400]	[400-600]	[600-]
Count	2820	1593	351	115	10	0	1	1	0	0

Table 4. Contamination analysis result data of 0.15 gr rGO-AgNPs

Interval	1	2	3	4	5	6	7	8	9	10
Max diameter (µm)	[0-5]	[5-15]	[15-25]	[25-50]	[50-100]	[100-150]	[150-200]	[200-400]	[400-600]	[600-]
Count	706	551	228	171	41	9	0	0	0	0

Table 5. Contamination analysis result data of 0.20 gr rGO-AgNPs

Interval	1	2	3	4	5	6	7	8	9	10
Max diameter (µm)	[0-5]	[5-15]	[15-25]	[25-50]	[50-100]	[100-150]	[150-200]	[200-400]	[400-600]	[600-]
Count	3293	1697	517	357	112	19	2	1	0	0

Based on the results of the 3D printing of dog bone specimens for the tensile test, it was evident that both pure PLA and PLA mixed with 0.10 g of rGO-AgNPs were uniformly distributed. However, when it came to cylindrical specimens, the uneven distribution was caused by contaminating particles, particularly between the nanocomposite and the resin. Before sonication, the nanocomposite was manually crushed, but it was discovered that a small number of nanocomposite particles were not perfectly smooth. Nevertheless, the PLA resin and nanocomposites were thoroughly mixed. To prevent bubbles from affecting the 3D printing results, the resin was meticulously mixed with a glass stirring rod. In the future, it will be crucial to use a specific mixture to obtain better results. Although the results of 3D printing indicated that the 0.10 g rGO-AgNPs nanocomposite particles were evenly distributed, digital microscopy revealed the presence of a few small particles that were not uniformly distributed. Achieving a completely uniform distribution of results can be challenging, especially considering its application in tissue engineering; however, this can be improved. Additionally, the more nanocomposites added to the resin, the greater the impact on color density, particularly for the black color of 0.20 g rGO-AgNPs. It needs to be verified that digital light can efficiently project each layer.

3.3. Mechanical Properties

The mechanical test was conducted using a 313 Family Universal Test Machine with a digital controller at Lab A (Material Selection), Sampoerna University. This machine is suitable for performing tension, bend, and compression tests with forces of up to 50 kN. The tensile test, a standard procedure for obtaining the stress-strain graph of a material, involves applying a static load in a uniaxial direction to a material specimen. The universal testing machine comprises two main parts: the loading unit and the control unit. The test specimen was secured in the loading unit, and the test results were obtained from the control unit. The flexural test specimens were manufactured using a DLP 3D printer, with dimensions of 2.5 × 6.0 × 115 mm, following the ASTM-D 638 standard at a test speed of 5 mm·min-1 (Feng et al., 2019; Tran et al., 2018).

The tensile tests were conducted to investigate the mechanical properties of the rGO-AgNPs scaffolds, and the resulting compressive stress-strain curves are depicted in **Figure 13**.

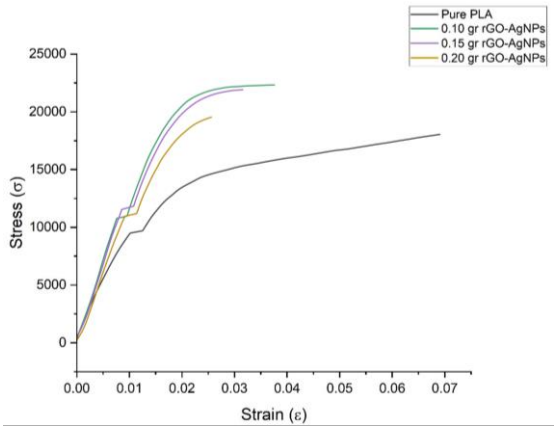

Figure 13. PLA and rGO-AgNPs stress-strain curves

The mechanical properties of a scaffold are crucial as they provide physical support for cell growth and migration. The presence of bubbles can alter the material's mechanical characteristics. Despite efforts to remove bubbles, they can still be present when casting liquid resin into a mold. Manual stirring with a glass rod is employed to minimize bubble formation. The scaffolds can be mechanically characterized by measuring parameters such as the modulus of elasticity and maximum strain. Young's modulus was calculated using the linear elastic regions of the stress-strain curves (**Figure 13**). Notably, rGO-AgNPs exhibited a significant decrease in the stress-strain curve. From the figure above, it can be concluded that the tensile strength increases as the amount of rGO-AgNPs decreases.

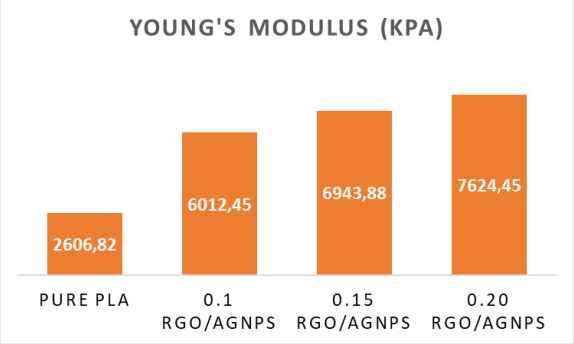

Figure 14. Young's modulus of obtained materials

The number of specimens can be seen in **Table 5**. The results of Young's modulus (**Figure 14**) of rGO-AgNPs are much higher than those of pure PLA. Pure PLA has a Young's modulus of 2606.82 kPa, 0.10 gr rGO-AgNPs has 6012.45 kPa, 0.15 gr rGO-AgNPs has 6943.88 kPa, and 0.20 gr rGO-AgNPs has 7624.45 kPa. The stiffness of a final product is determined by the material's elasticity. A low stiffness of the osteoconductive scaffold can lead to morphological changes and deformation of the internal porous structure, affecting the shape and structure of the new bone tissue that grows within the pores. A material with a higher Young's modulus is less elastic and more resistant to deformation. To enhance the mechanical properties, fillers can be added to the polymer matrix, or nanocomposites with strong mechanical properties, such as graphene, can be employed. Adding graphene to the resin could improve its mechanical characteristics, while silver nanoparticles could impart antimicrobial properties to polymer scaffolds. As shown in the previous figures, specimens containing rGO-AgNPs exhibited a greater modulus than others. Thus, the material with the highest modulus of elasticity is 0.20 gr of rGO-AgNPs. However, achieving a uniform dispersion was still challenging. The synergistic dispersion of rGO-AgNPs enhanced the efficiency of stress transfer within the matrix, resulting in a synergistic effect on the mechanical reinforcement of the polymer scaffolds.

4. CONCLUSION

In this study, the rGO-AgNPs nanocomposites are successfully synthesized. XRD Measurements were carried out to further characterize the synthesized results of rGO-AgNPs. The XRD spectrum indicates diffraction peaks at 38.14°, 44.30°, 64.50°, and 77.42°. These peaks were corresponding to the (111), (200), (220), and (3111) planes of the Ag crystals, respectively. The surface results from microscope observation for pure PLA and PLA mixed with 0.10 gr rGO-AgNPs showed that the sample's surfaces were uniformly distributed. The results from the tensile test showed that rGO-AgNPs had higher tensile strength. The tensile strength increases as the number of rGO-AgNPs decreases. The results of young's modulus from pure PLA to rGO-AgNPs showed a steady increase. Therefore, specimens containing rGO-AgNPs exhibited a greater modulus than others.

REFERENCES

Affi, J., Handayani, M., Anggoro, M.A., Esmawan, A., Sabarman, H., Satriawan, A., Shalannanda, W., Siburian, R. & Anshori, I. (2023) Electrochemical and capacitive behavior of reduced graphene oxide from green reduction of graphene oxide by urea for supercapacitor electrodes. Journal of Materials Science: Materials in Electronics, 34:1638.

Bai, R.G., Muthoosamy, K., Manickam, S. & Hilal-Alnaqbi, A. (2019) Graphene-based 3D scaffolds in tissue engineering: fabrication, applications, and future scope in liver tissue engineering. International journal of nanomedicine, 14:5753.

Basak, M., Rahman, M.L., Ahmed, M.F., Biswas, B. & Sharmin, N. (2022) The use of X-ray diffraction peak profile analysis to determine the structural parameters of cobalt ferrite nanoparticles using Debye-Scherrer, Williamson-Hall, Halder-Wagner and Size-strain plot: Different precipitating agent approach. Journal of Alloys and Compounds, 895:162694.

Ciptasari, N.I., Handayani, M., Kaharudin, C.L., Afkauni, A.A., Hatmanto, A.D., Anshori, I., Maksum, A., Riastuti, R. & Soedarsono, J.W. (2022) Synthesis of Nanocomposites Reduced Graphene Oxide-Silver Nanoparticles Prepared by Hydrothermal Technique Using Sodium Borohydride as a Reductor for Photocatalytic Degradation of Pb Ions in Aqueous Solution. Eastern-European Journal of Enterprise Technologies, 6/5(120):54-62.

Feng, Z., Li, Y., Hao, L., Yang, Y., Tang, T., Tang, D. & Xiong, W. (2019) Graphene-reinforced biodegradable resin composites for stereolithographic 3D printing of bone structure scaffolds. Journal of Nanomaterials, 2019.

Fernando, S.S.N., Gunasekara, T.D.C.P. & Holton, J. (2018) Antimicrobial Nanoparticles: applications and mechanisms of action.

Handayani, M., Kepakisan, K.A.A., Anshori, I., Darsono, N. & Thaha, Y.N. (2021) Graphene oxide-based nanocomposite modified screen printed carbon electrode for qualitative cefixime detection. In AIP Conference Proceedings (Vol. 2382, No. 1, p. 040005). AIP Publishing LLC.

Handayani, M., Suwaji, B.I., Ihsantia Ning Asih, G., Kusumaningsih, T., Kusumastuti, Y., Rochmadi & Anshori, I. (2022) In-situ synthesis of reduced graphene oxide/silver nanoparticles (rGO/AgNPs) nanocomposites for high loading capacity of acetylsalicylic acid. Nanocomposites, 8(1):74-80.

Jakus, A.E., Secor, E.B., Rutz, A.L., Jordan, S.W., Hersam, M.C. & Shah, R.N. (2015) Three-dimensional printing of high-content graphene scaffolds for electronic and biomedical applications. ACS nano, 9(4):4636-4648.

Liu, J., Cui, L. & Losic, D. (2013) Graphene and graphene oxide as new nanocarriers for drug delivery applications. Acta biomaterialia, 9(12):9243-9257.

Sayyar, S., Officer, D.L., & Wallace, G.G. (2017) Fabrication of 3D structures from graphene-based biocomposites. Journal of Materials Chemistry B, 5(19):3462-3482.

Shadjou, N., Hasanzadeh, M. & Khalilzadeh, B. (2018) Graphene based scaffolds on bone tissue engineering. Bioengineered, 9(1):38-47.

Shin, S.R., Li, Y.C., Jang, H.L., Khoshakhlagh, P., Akbari, M., Nasajpour, A. & Khademhosseini, A. (2016) Graphene-based materials for tissue engineering. Advanced drug delivery reviews, 105:255-274.

Singh, Z. (2016) Applications and toxicity of graphene family nanomaterials and their composites. Nanotechnology, science, and applications, 9:15.

Silva, M., Alves, N.M. & Paiva, M.C. (2018) Graphene-polymer nanocomposites for biomedical applications. Polymers for Advanced Technologies, 29(2):687-700.

Tran, T.T., Hamid, Z.A. & Cheong, K.Y. (2018) A review of mechanical properties of scaffold in tissue engineering: aloe vera composites. In Journal of Physics: Conference Series (Vol. 1082, No. 1, p. 012080). IOP Publishing.

Zheng, X., Zhang, P., Fu, Z., Meng, S., Dai, L. & Yang, H. (2021) Applications of nanomaterials in tissue engineering. RSC Advances, 11(31):19041-19058.